UNIVERSITY OF WISCONSIN

CENTER FOR PLASMA THEORY AND COMPUTATION

REPORT

Helical Post Stellarator

(Part 1: Vacuum Configuration)

P. E. Moroz

Center for Plasma Theory and Computation
Department of Engineering Physics
University of Wisconsin, Madison, Wisconsin 53706-1687

August 1997

UW-CPTC 97-15

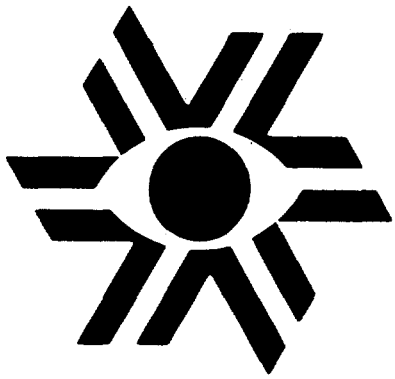

MADISON, WISCONSIN 53706-1687

HELICAL POST STELLARATOR

(Part 1: Vacuum Configuration)

by

P. E. Moroz

Center for Plasma Theory and Computation

Department of Engineering Physics

University of Wisconsin, Madison, WI 53706, USA

August 1997

UW-CPTC 97-15

HELICAL POST STELLARATOR

(Part 1: Vacuum Configuration)

Paul E. Moroz

Center for Plasma Theory and Computation

Department of Engineering Physics

University of Wisconsin, Madison, WI 53706, USA

ABSTRACT.

Results on a novel type of stellarator configuration, the Helical Post Stellarator (HPS), are presented. This configuration is different significantly from all previously known stellarators due to its unique geometrical characteristics and unique physical properties. Among those are: the magnetic field has only one toroidal period (M =1), the plasma has an extremely low aspect ratio, A ≈ 1, and the variation of the magnetic field, B, along field lines features a helical ripple on the inside of the torus. Among the main advantages of a HPS for a fusion program are extremely compact, modular, and simple design compatible with significant rotational transform, large plasma volume, and improved particle transport characteristics.

I. Introduction.

Traditionally, stellarators are large aspect ratio machines with an aspect ratio A (which is the ratio of the average major radius, R, to the average minor radius, r, for the last closed flux surface) around 10. The so-called low-A stellarators [1] have an aspect ratio $A \approx 5 - 7$. The lowest-A stellarators ever built are the Compact Helical System (CHS) [2], the Compact Auburn Torsatron (CAT) [3], and the heliac H-1 [4], which have $A \approx 5$. One of the advantages of the low-A stellarators, the high-β regime, was demonstrated by the experiments on CHS [2], where the record values of volume average $\langle\beta\rangle \approx 2.1\%$, reached so far in stellarators, have been reported.

In parallel to the development of the world Spherical Tokamak (ST) program [5-13], which promises more compact, higher β, and a less disruptive approach for tokamaks, the Spherical Stellarator (SS) program has been initiated recently [14-22] for machines with stellarator features and an aspect ratio A below 3.5. The SS concept offers a significantly different (from traditional stellarator or tokamak approaches) way to a fusion reactor, which can be envisioned as a compact and inexpensive machine with the steady-state, high-β, and strong bootstrap current regimes of operation. From that point of view, a few simple and principally different SS configurations have been recently considered: SS with a straight center post [14], with planar coils [18], and with outboard stellarator windings [19]. Various combinations of these main types can result in a more general modular twisted coil approach and might correspond to parameter optimization [16-17, 20-21]. It was shown [15, 20, 22] that a plasma current via inductive drive or bootstrap effect is advantageous in the SS for reaching higher β equilibria and improved transport characteristics.

The present paper introduces a principally new type of SS configuration which we call the Helical Post Stellarator (HPS). The HPS configuration is so unusual that it sets a few records

for stellarators. First of all, to our knowledge, this is the first stellarator configuration ever considered with a single toroidal field period (M=1). Also, this configuration does not have the traditional stellarator helical windings or twisted coils encircling the plasma, and the only helical element of the HPS configuration is a helical post located in the center of the torus. The plasma aspect ratio, $A \approx 1$, obtained in HPS configurations is also out of the range ever considered for stellarators. A relatively large rotational transform, $\iota \approx 0.1 - 0.15$, obtained for these extremely low aspect ratios and inboardly located helical ripple represent the significant advantages of these configurations. Taking into account all these factors together with the extreme simplicity of the coil system makes an HPS to be of a particular interest for fusion applications.

The neoclassical transport theory in stellarators has been developed first [23-24] for a simple magnetic field model,

$$B / B_o = 1 - \varepsilon_t \cos\theta - \varepsilon_h \cos\eta, \qquad (1)$$

where B_o is the central magnetic field, $\eta = m\theta - nN\varphi$, m and n are the poloidal and toroidal mode numbers, N is the number of toroidal field periods, and θ and φ are the poloidal and toroidal angles. This model field includes just the main toroidal and helical harmonics caused by the toroidicity and helical windings. The theory predicts significant particle and energy fluxes in the low collisionality $1/\nu$ regime, which are proportional to $\varepsilon_t^2 \, \varepsilon_h^{3/2} / \nu$, with ν being the collision frequency. However, the real stellarators usually have significantly more complicated spectrum of helical harmonics than that given by Eq. (1). As it was first found numerically via the Monte Carlo simulations [25], additional helical harmonics can significantly improve the transport characteristics of a stellarator. Theoretical analysis and Monte Carlo calculations of Ref. 26 explained this effect by considering a more complicated model field.

$$B = B_o [1 - \varepsilon_t \cos\theta - \varepsilon_h \cos\eta (1 - \sigma\cos\theta)], \qquad (2)$$

which is different from (1) in case of non-zero σ. It was found, that for $\sigma \approx \varepsilon_h/\varepsilon_t \approx 1$, the radial drift of the helically trapped particles is reduced significantly, and numerical example has demonstrated the reduction of neoclassical diffusion by an order of magnitude in comparison with the case of $\sigma = 0$ and the same ε_t and ε_h . Later theory and numerical calculations [27, 28] generalized and confirmed these results for configurations with multiple poloidal harmonics. The main conclusion was the same - an order of magnitude reduction of neoclassical transport coefficients is possible if the helical ripple is localized inboard of the torus.

For low-aspect-ratio stellarators in general, and especially for SS configurations where both ε_t and ε_h are significant and of the order of 1, neoclassical transport can be, in principle, very poor and requires careful optimization. Taking into account the above mentioned facts, we were searching for an SS configuration that had an inboardly located magnetic ripple. The HPS system, discussed below, gives a simple, interesting and unusual example of such a configuration.

The rest of the paper is organized as follows. In Section II, the coil system of HPS is described. In Section III, the main parameters of the vacuum magnetic field configuration without PF rings are given, and Section IV demonstrates similar results for a configuration with PF rings. The neoclassical transport and the S-factor are discussed in Section V. Finally, the main conclusions are summarized in Section VI.

II. Coil system of the HPS

The HPS coil configuration can be obtained from a typical ST coil systems [5] by replacing the straight center post of an ST with the helical post, as shown in Fig. 1. The outboard parts of TF coils can be the same as in an ST and, in principle, can even be replaced by the solid conducting wall to reduce the outboard magnetic field ripple. Consequently, the total current of all TF coils goes through a single helical center post (HCP), or equivalently, through the number of close conductors of a HCP. Similar to modifying an ST, the HPS can be obtained by replacing the straight center post of an SS configuration of Refs. 14-15 with the HCP. In this paper, however, we will consider only the first option (modification of an ST), while the second option (modification of an SS) will be discussed elsewhere.

The configuration presented in Fig. 1 corresponds to the first round of the coil system optimization regarding the extreme low aspect ratio, large enclosed volume, large vacuum rotational transform, small outboard magnetic field ripple, and small magnetic island structure. The coil system shown includes 12 outboard (half-elliptical) TF coils, 3 pairs of the poloidal field (PF) rings, and a single HCP making 1.5 turns around the vertical axis ($\Delta\varphi_{cp} = 3\pi$). The winding law for the HCP presented in figures in this paper was chosen as

$$\varphi = \frac{\Delta\varphi_{cp}}{2} \sin\left(\frac{\pi z}{2H}\right)$$
$$R = R_{cp}\,(1 - \zeta^2)^2 \qquad (3)$$

where φ is the toroidal angle, z is the distance from the equatorial plane, R is the distance from the vertical axis (major radius), H is the half-height of the HCP, and the parameter ζ = 0 for $|z| \le h$, and $\zeta = (|z| - h)/(H - h)$ for $h < |z| \le H$, with h being the half-length of the central part of the HCP. The dimensions chosen for an example of a system with good parameters are: $R_{cp} = 0.1$ m, $h = 0.6$ m, and $H = 0.75$ m.

A set of 3 pairs of PF rings, shown in Fig. 1, is not a necessary element for forming the vacuum flux surfaces. It is, however, advantageous for shaping the flux surfaces, optimizing the magnetic ripple, adjusting the plasma aspect ratio and controlling the plasma location. It will be useful also for reaching high β in the regimes with the finite plasma pressure and finite plasma current.

III. HPS magnetic field configuration without PF rings.

Tracing along field lines, carried out via the UBFIELD code (see, for example [29]) for the coil configuration and parameters discussed in the previous section, demonstrates a number of peculiar characteristics of the HPS magnetic field. First we discuss the configuration without PF rings.

The closed vacuum flux surfaces of large volume are shown in Figs. 2, 3 for two perpendicular cross-sections of the device, respectively in X-Z and Y-Z planes of the Cartesian coordinate system with Z being the vertical axis, and X-Z plane corresponding to $\varphi = 0$ and $\varphi = \pi$. The cross-sections of outboard parts of the TF coils and the HCP are presented in these figures as well. The Poincare puncture plots calculated for a large number of closed flux surfaces demonstrate that the enclosed area is practically island-free, although the narrow chains of magnetic islands are present for flux surfaces where rotational transform, ι, goes through the rational value, such as 1/8, 1/9, 1/10, etc. These magnetic islands are too narrow to affect the plasma confinement in the HPS. Still, the finite β calculations for magnetic islands should be, probably, carried out before the actual high-β experiment will be designed. The aspect ratio of the configuration presented is extremely low, $A \approx 1.17$, which has never been considered before for stellarators. The dashed curves

in Figs. 2, 3 demonstrate the geometry of the opened field lines. These field lines go along the HCP and might serve as a part of the divertor system with the divertor plates conveniently located at the top and bottom parts of an HPS, where the free space is readily available (see Fig. 4, which shows schematically the whole coil configuration together with three main plasma cross-sections.)

The perspective view of the coil system and the last closed vacuum flux surface is given in Fig. 5. One can see the periodic modulation induced by the 12 TF coils and that the last flux surface extends further in the space between the TF coils. This effect is similar to that in a tokamak or in any other toroidal configuration with the finite number of TF coils and is caused by the proximity of the flux surface to the TF coils. The corresponding outboard magnetic ripple (see Fig. 6a for the last closed flux surface, $\rho = 1$, where ρ is the normalized average minor radius) might increase the transport coefficients significantly and thus should be avoided. This ripple is reduced significantly for the internal flux surfaces, and Fig. 6b demonstrates, as an example, that it is practically absent for a flux surface with $\rho = 0.5$. The same 12-period modulation can be seen in Fig. 7a showing $|B|$ distribution on the flux surface, $\rho = 1$. There, B_0 designates the value of the first solid-line contour, and ΔB is the difference between the adjacent contour lines. Solid contours correspond to $|B| \geq B_0$, while the dotted ones correspond to $|B| < B_0$. The $|B|$ bumpiness is not seen for the flux surface $\rho = 0.5$ (Fig. 7b), where the helical symmetry of $|B|$ on the inboard changes to the toroidal symmetry on the outboard of the flux surface. A few methods can be used to reduce the outboard ripple which are mainly based on moving the plasma further from the outboard parts of TF coils or on increasing their number. To accomplish the former, the additional divertor coils or limiters can be used, or the vertical magnetic field produced by PF rings can be imposed to move the plasma closer to the center.

The equatorial (Z = 0) cross-section of the plasma is given in Fig. 8 where cross-sections for TF coils and for the HCP are presented as well. The magnetic axis projection is shown by the dashed curve, which seems as circular although being non-planar in reality. The helical space around the HCP is free of plasma and naturally prevents the HCP conductors from contacts with the hot plasma. In calculations of the magnetic field, presented in Figs. 6 and 7, the total current through the HCP was I_{cp} = 600 kA which allowed obtaining magnetic field magnitudes of up to 1T. This fact demonstrates the high efficiency of the HPS coil system capable of producing high magnetic fields at moderate currents in the coils.

Radial dependence of the rotational transform, $\iota = 1/q$ (q being the safety factor), is shown in Fig. 9 (solid curve) and varies from 0.123 at the axis to 0.055 at the plasma edge. From the point of view traditional large-aspect-ratio stellarators, which often have $\iota \sim 1$, such rotational transform is small. However, for an extreme-low-aspect-ratio machine considered, it is a high value. Actually, these values of ι, found for the HPS without any plasma current, are only a factor of two lower than that considered for stable regimes in spherical tokamaks with the large plasma current [11].

IV. HPS magnetic field configuration with PF rings.

As it was mentioned above, the PF rings should be remained as an important element of the HPS coil system to control both the vacuum magnetic field configuration and the configuration at finite plasma pressure and finite plasma current. Here we show that small currents in PF rings (about 4 kA each, which is small in comparison with I_{cp} = 600 kA) can be used effectively to reduce the outboard magnetic ripple and control the aspect ratio of the vacuum magnetic configuration.

Location of the PF rings in this example can be seen in Fig. 10, where the TF-coil and the HCP projections are sketched, as well, and the main cross-sections of the last closed vacuum flux surface are shown. In this case, the plasma is shifted inboard and is more vertically elongated. The plasma aspect ratio is A = 1. The corresponding perspective view of the coil system and the last closed flux surface is given in Fig. 11, which demonstrates rather well a near spherical-shaped plasma of the HPS with a modest central opening through which the HCP extends. The puncture tracing of the large number of closed flux surfaces is given in Fig. 12 (for X-Z cross-section) and Fig. 13 (for Y-Z cross-section). It demonstrates clearly the absence of significant magnetic islands in the HPS configuration considered.

The radial dependence of the rotational transform is shown in Fig. 9 by the dashed curve. It varies from $\iota(0) = 0.15$ to $\iota(1) = 0.045$ and for the most of the plasma volume it is larger than for the case without the PF rings.

Magnetic field variation along the field line, for the last closed flux surface, is shown in Fig. 14a. Because of the plasma for this case is pushed inward, the magnetic field magnitude increases and reaches $B_{max} = 1.7$ T for the same current in the center post of 600 kA. Thus, the efficiency of the coils is even higher. The outboard magnetic ripple is also significantly reduced. Further reduction of the outboard ripple (practically, its total elimination) can be obtained with the increased number of TF coils to N = 24 (Fig. 14b).

V. Neoclassical transport at low collisionality.

Neoclassical particle and energy fluxes in stellarators (see, for example, [27-28]) at low collisionality ($1/\nu$ regime) can be expressed through the geometrical factor, S, first considered in [27]. Let us present this factor for the general magnetic field of the form

$$B / B_o = \sum_{mn} \varepsilon_{mn} \cos(m\theta - nN\varphi) , \qquad (4)$$

used in our calculations, with $\varepsilon_{00} = 1$, where the index n = 0,1,2, etc., while the index m includes both negative and positive modes. This general form includes, as the particular cases, the model forms given by Eqs. (1) and (2). For that cases, $\varepsilon_t = -\varepsilon_{10}$ and $\varepsilon_h = -\varepsilon_{m_0,n_0}$, where m_o and n_o correspond to the main helical harmonic (usually, $n_o = 1$, which holds also for the HPS configuration considered). The factor, σ, in Eq. (2) comes from two equal neighboring poloidal harmonics $\varepsilon_{m_0+1,n_0} = \varepsilon_{m_0-1,n_0}$, so that $\sigma = -2\, \varepsilon_{m_0+1,n_0} / \varepsilon_{m_0,n_0}$. The θ and φ angles correspond to the Boozer coordinate system [30].

The parameter, S, for the general field of Eq. (4) can be defined as

$$S = \frac{1}{\rho^2} \int_0^{2\pi} d\theta\, \varepsilon_H^{3/2} \left[1.778 \left(\frac{\partial \varepsilon_T}{\partial \theta}\right)^2 - 2.133 \left(\frac{\partial \varepsilon_T}{\partial \theta}\right)\left(\frac{\partial \varepsilon_H}{\partial \theta}\right) + 0.684 \left(\frac{\partial \varepsilon_H}{\partial \theta}\right)^2 \right] \qquad (5)$$

where

$$\varepsilon_T = \sum_{m \neq 0} \varepsilon_{m0} \cos(m\theta) \qquad (6)$$

$$\varepsilon_H = \sqrt{\left(\sum_m \varepsilon_{mn_0} \cos(m\theta)\right)^2 + \left(\sum_m \varepsilon_{mn_0} \sin(m\theta)\right)^2} \qquad (7)$$

To judge how good the configuration is optimized for transport, it is useful to compare the S-factor given by Eq. (5) with the factor S_o calculated for the same configuration but including only the first term in the square brackets (so, the cancellation caused by the terms with different signs, or enhancement, in an unfavorable case, cannot be realized):

$$S_o = \frac{1.778}{\rho^2} \int_0^{2\pi} d\theta \, \varepsilon_H^{3/2} \left(\frac{\partial \varepsilon_T}{\partial \theta} \right)^2 \qquad (8)$$

For the model field of Eq. (2), the ratio, S/S_o, can be written in the form

$$\frac{S}{S_o} = \frac{\int_0^{2\pi} d\theta \, \sin^2\theta \, |1-\sigma \cos\theta|^{3/2} \left(1 - 1.2\sigma p + 0.385\sigma^2 p^2\right)}{\int_0^{2\pi} d\theta \, \sin^2\theta \, |1-\sigma \cos\theta|^{3/2}} \qquad (9)$$

where $p = \varepsilon_h / \varepsilon_t$. The integrals in Eq. (9) can be easily computed and the results are presented in Figs. 15 and 16. Fig. 15 shows contours of S/S_o as a function of σ and p, with solid lines designating the contours with $S/S_o \geq 1$, and dashed ones - with $S/S_o < 1$. The difference between neighboring contours is 0.15. Location of the minimum, which is about 0.066, is shown by the dash-dot lines. Fig. 16 presents the same data but only for four different values of the parameter p: 1.5, 1, 0.5 and 0.25. The main conclusion that one can make from these figures is that in a situation, when the main helical harmonic is small (p is small), additional harmonics cannot improve or degrade the transport significantly. In an opposite situation with the large p, however, additional harmonics have dramatic effect on transport which can be improved (for this model field) by a factor of 15. On the other hand, improper choice of additional harmonics in this case can degrade the particle transport significantly, as well.

The S-factor calculations for the HPS configurations of Sections III and IV are presented in Fig. 17, where the radial dependence of S/S_o is shown. One can see the reduction of the parameter S, in comparison with S_o, up to the factor of 4, which reflects the corresponding

improvement of the collisionless particle transport. Further optimization of the HPS configuration by adjusting the currents in the coils or modifying the HCP winding law might, probably, improve this factor and bring it closer to that discussed above for the model field (2) with optimized parameters.

VI. Discussion and conclusions.

A novel stellarator configuration. the Helical Post Stellarator, is presented. This configuration has a number of features which are very unique and very unusual in comparison with that of the presently known stellarators. Thus, the HPS holds a few records for stellarators. To our knowledge, this is the only configuration having just a single toroidal period.

The HPS coil system is efficient for production of the strong magnetic fields in the plasma at moderate currents in the coils, which is similar to an ST and corresponds to the extreme low plasma aspect ratios, $A \approx 1$. The major radius of some places within the plasma volume can reach $R = 0$, which also represents a record not only for stellarators but for the other toroidal devices. Effective control over the plasma location, magnetic field magnitude and magnetic ripple can be accomplished by the system of PF rings with very moderate currents, although the configuration of interest can be obtained even without the PF rings.

The only helical element of the HPS is the helical center post which produces stellarator magnetic fields with the magnetic ripple located inboard. Theoretically, it was shown [26-28] that such type of harmonic composition is the most efficient for collisionless plasma confinement. Our calculations of the S-factor for the HPS confirmed this conclusion.

To eliminate the outboard magnetic ripple, which might be dangerous for particle transport, the number of outboard parts of the TF coils is recommended to be large. In this regard, the solid conducting shell replacing the TF coils can be considered as an interesting option.

The rotational transform produced in the HPS is rather high for such low aspect ratios and reaches the values of 0.12 - 0.15. Also, the rotational transform is a decreasing function of the minor radius, similar to that in an ST, or in the SS configurations considered before [11-19]. This is convenient for adding the plasma current to the system. Actually, the HPS is featuring the most compact and the most spherical plasma among all SS configurations, and thus can be considered as a new member of the Spherical Stellarator family.

One more advantage of the HPS is the simplicity of the coil system, with the HCP being the major technological element. The HPS can be easily built from the corresponding ST by replacing the straight center post with the HCP. For a reactor, if necessary, the HCP can be made removable, as it is proposed for a center post in an ST [12-13].

The HPS has a potential to resolve a few problems of the ST approach. One of them is the steady-state operation which is problematic for an ST but is natural for an HPS as a stellarator device. Another severe problem of an ST-reactor is the strong heat flux to the center post from the plasma being practically in the direct contact with the center post structure. Opposite to that, the plasma in the HPS is separated from the HCP by the divertor region from where the energetic particles leaving the plasma can be removed before they reach the HCP. These particles follow the field lines to the top and bottom regions where the toroidally symmetric divertor plates can be conveniently installed.

This paper introduces the HPS configuration and presents the results for its vacuum magnetic field structure and properties. The results on the finite plasma pressure and finite plasma

current equilibrium calculations for the HPS are planned to be presented in a separate publication.

In conclusion, the author would like to acknowledge useful discussions of various related questions with S. P. Hirshman. This work was supported by the U.S. DOE Grant No. DE-FG02-97ER54395.

References

[1] J. F. Lyon, B. A. Carreras, V. E. Lynch et al., Fusion Technology **15** (1989) 1401.

[2] S. Okamura, K. Matsuoka, K. Nishimura et al., Nucl. Fusion 35 (1995) 283.

[3] S. F. Knowlton, R. F. Gandy, J. D. Hanson et al., Journ. Fusion Energy **12** (1993) 261 .

[4] B. D. Blackwell, G. G. Borg, R. L. Dewar et al., Proc. 15th Int. Conf. on Plasma Phys. and Contr. Nucl. Fusion Res., Seville 1994 (International Atomic Energy Agency, Vienna 1995) Vol. **2**, p. 337.

[5] A. Sykes, Plasma Phys. Contr. Fus. **36** (1994) B93.

[6] M. Ono et al., Proc. Int. Conf. on Plasma Phys. & Contr. Fus. Res., Wurzburg 1992 (International Atomic Energy Agency, Vienna 1993) Vol. **1**, p. 693.

[7] A. K. Martin, T. R. Jarboe, Plasma Phys. Contr. Fusion **38** (1996) 1967.

[8] M. Peng, M. Ono, S. Kaye, R. Goldston, Bull. Am. Phys. Soc. **41** (1996) 1403.

[9] V. E. Golant et al., IAEA-CN-64/GP-15, 16th IAEA Conf. on Plasma Phys. and Contr. Nucl. Fus. Res., Montreal (1996).

[10] R. Fonck et al., Bull. Am. Phys. Soc. **41** (1996) 1400.

[11] Y.-K.M. Peng, R.J. Colchin, C.L. Hedrick et al., Proc. 15th Int. Conf. of Plasma Phys. and Contr. Fus. Res., Seville 1994 (International Atomic Energy Agency, Vienna 1995) Vol. **2**, p. 643.

[12] I.N. Sviatoslavsky, E.A. Mogahed, Y.-K. M. Peng et al., Fusion Technology **30** (1996) 1649.

[13] D.C. Robinson, R. Buttery, I. Cook et al., Fusion Technology **30** (1996) 1360.

[14] P. E. Moroz, Phys. Rev. Lett. **77** (1996) 651.

[15] P. E. Moroz, Physics of Plasmas **3** (1996) 3055.

[16] D. W. Ross, P. M. Valanju, H. He et al., Plasma Phys. Reports **23** (1997) 492.

[17] D. A. Spong, S. P. Hirshman, J. C. Whitson, Plasma Physics Reports **23** (1997) 483.

[18] P. E. Moroz, Plasma Physics Reports **23** (1997) 502.

[19] P. E. Moroz, Nucl. Fusion **37** (1997) No. 8.

[20] P. E. Moroz, D. B. Batchelor, B. A. Carreras et al., Fusion Technology **30** (1996) 1347.

[21] P. E. Moroz, D. B. Batchelor, B. A. Carreras et al., Bull. Amer. Phys. Soc. **41** (1996) 1567.

[22] P. E. Moroz, Stellarator News **48** (1996) 2.

[23] A. A. Galeev, R. Z. Sagdeev, H. P. Furth, M. N. Rosenbluth, Phys. Rev. Lett. **22** (1969) 511.

[24] J. W. Connor, R. J. Hastie, Phys. Fluids **17** (1974) 114.

[25] R. E. Potok, P. A. Politzer, L. M. Lidsky, Phys. Rev. Lett. **45** (1980) 1328.

[26] H. E. Mynick, T. K. Chu, A. H. Boozer, Phys. Rev. Lett. **48** (1982) 322.

[27] K. C. Shaing, S. A. Hokin, Phys. Fluids **26** (1983) 2136.

[28] V. E. Bykov, A. V. Georgievskij, V. G. Peletminskaya et al., Nucl. Fusion **24** (1984) 1195.

[29] P. E. Moroz, Phys. Plasmas **2** (1995) 4269.

[30] A. H. Boozer, Phys. Fluids **25** (1982) 520.

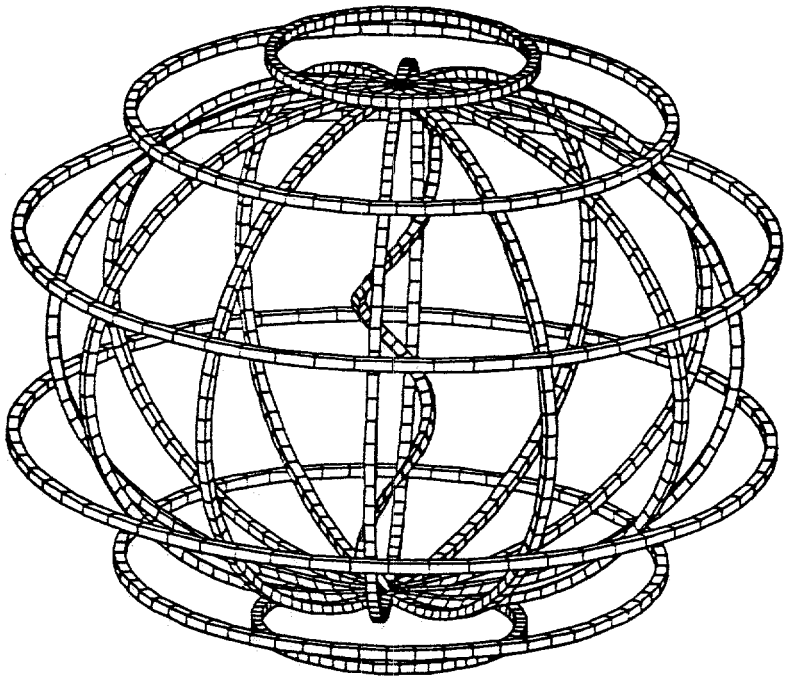

Fig. 1. An HPS coil system.

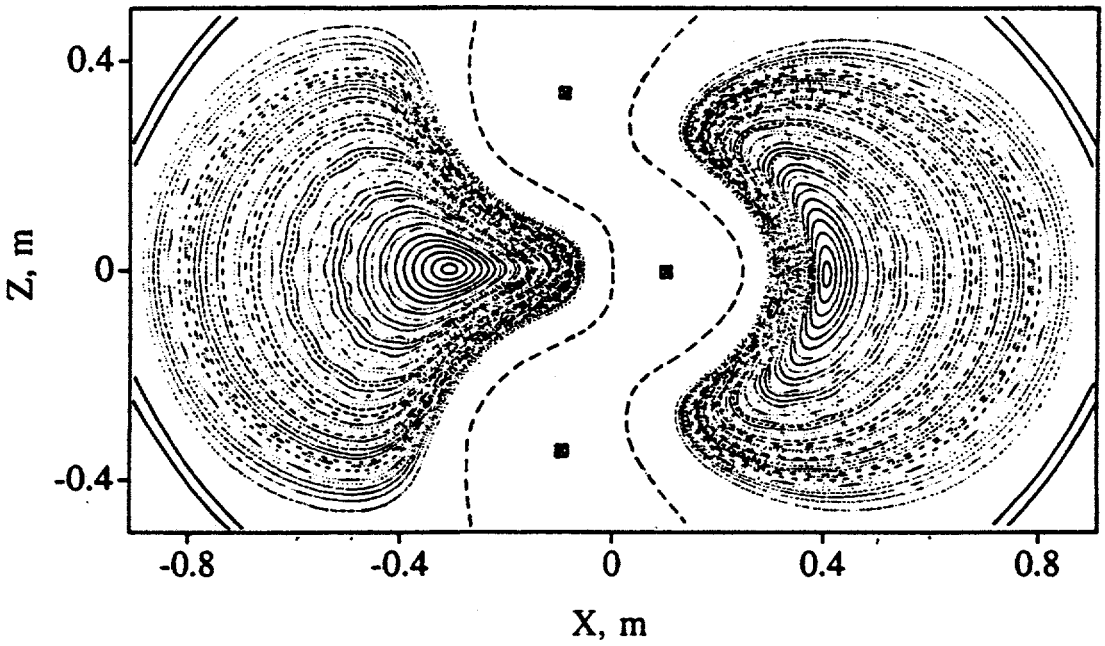

Fig. 2. Poincare puncture plots for closed vacuum flux surfaces in the X-Z cross-section. The dashed curves demonstrate the geometry of the opened field lines. Cross-sections of the coils are shown as well.

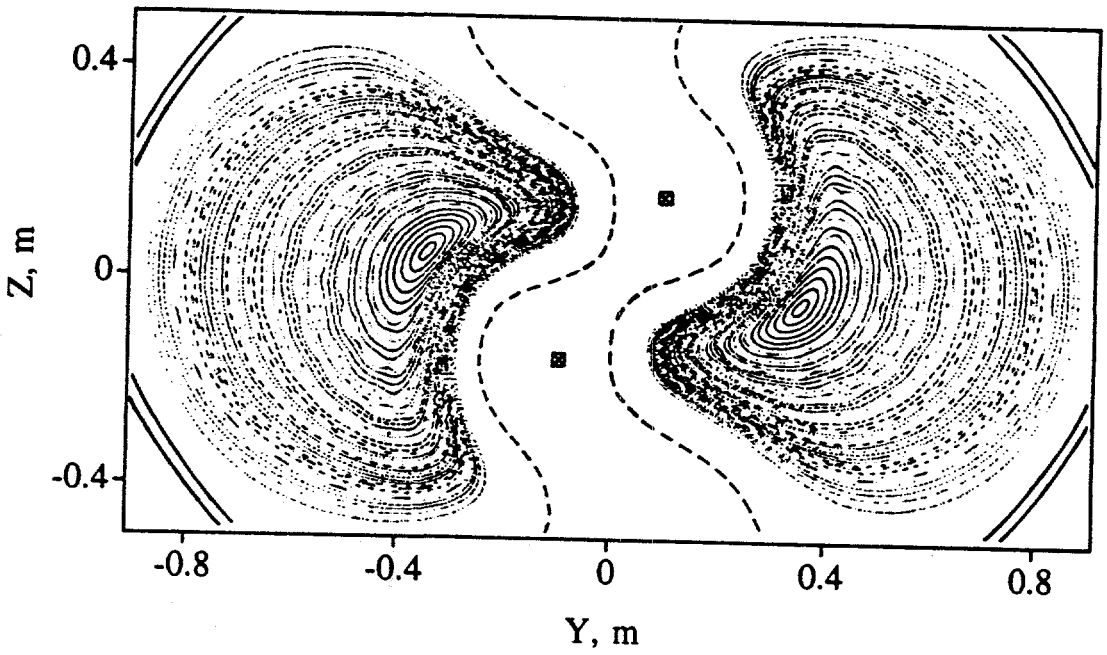

Fig. 3. Same as Fig. 2, but for the Y-Z cross-section.

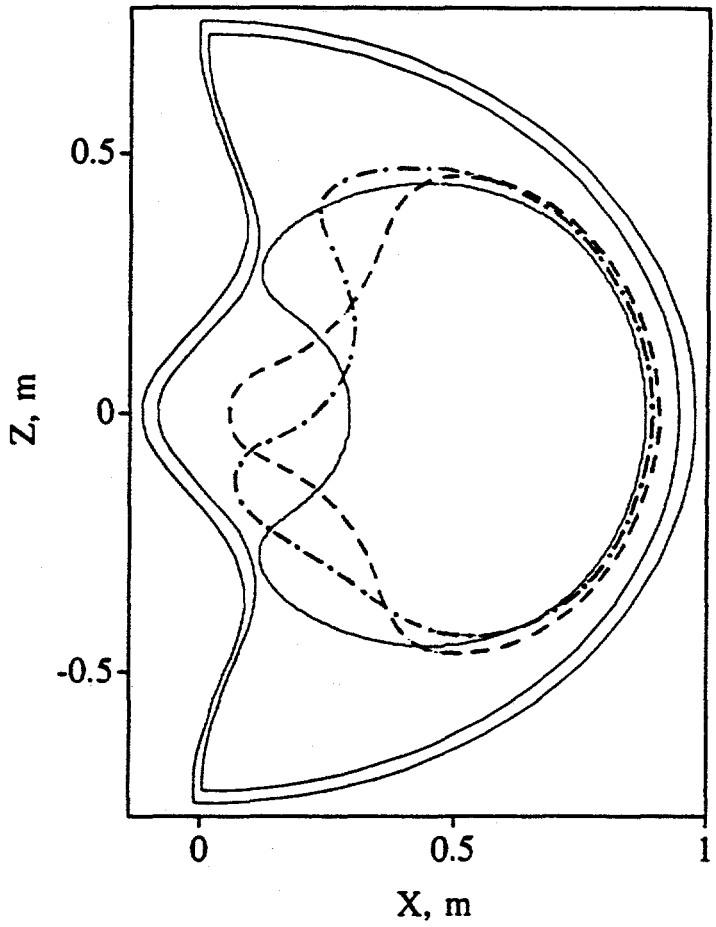

Fig. 4. Poloidal projection of the HPS coil system together with the main cross-sections of the last closed flux surface.

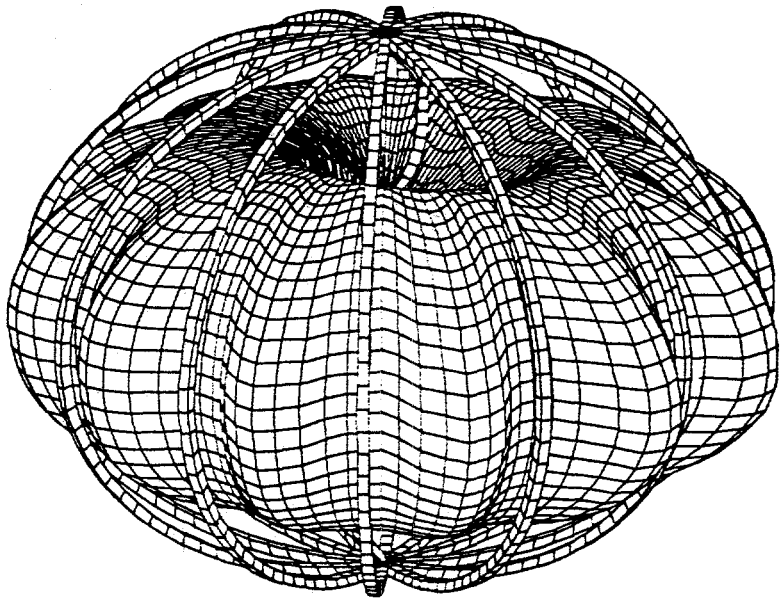

Fig. 5. Perspective view of the HPS plasma and the coils.

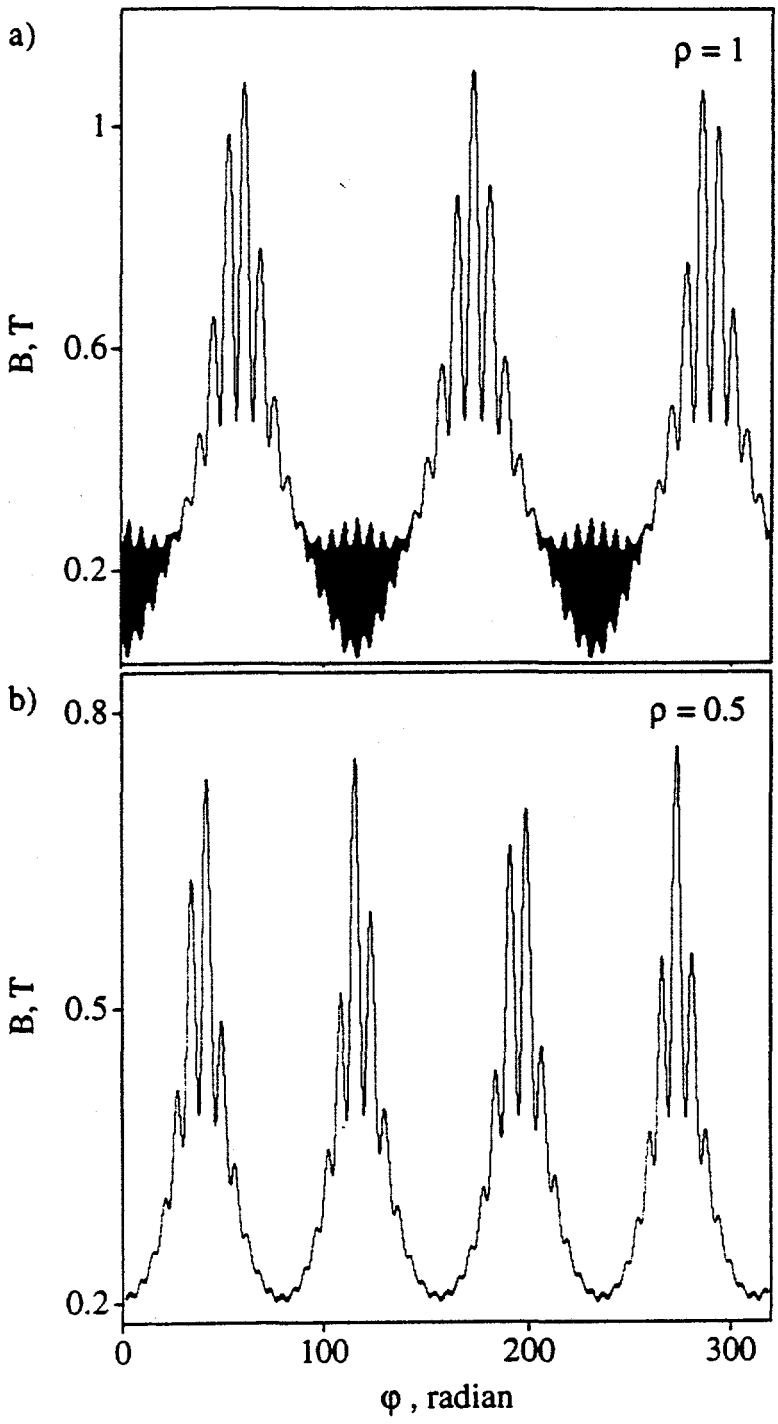

Fig. 6. Magnetic field variation along a field line, (a) for the last flux surface, $\rho = 1$; (b) for the flux surface, $\rho = 0.5$.

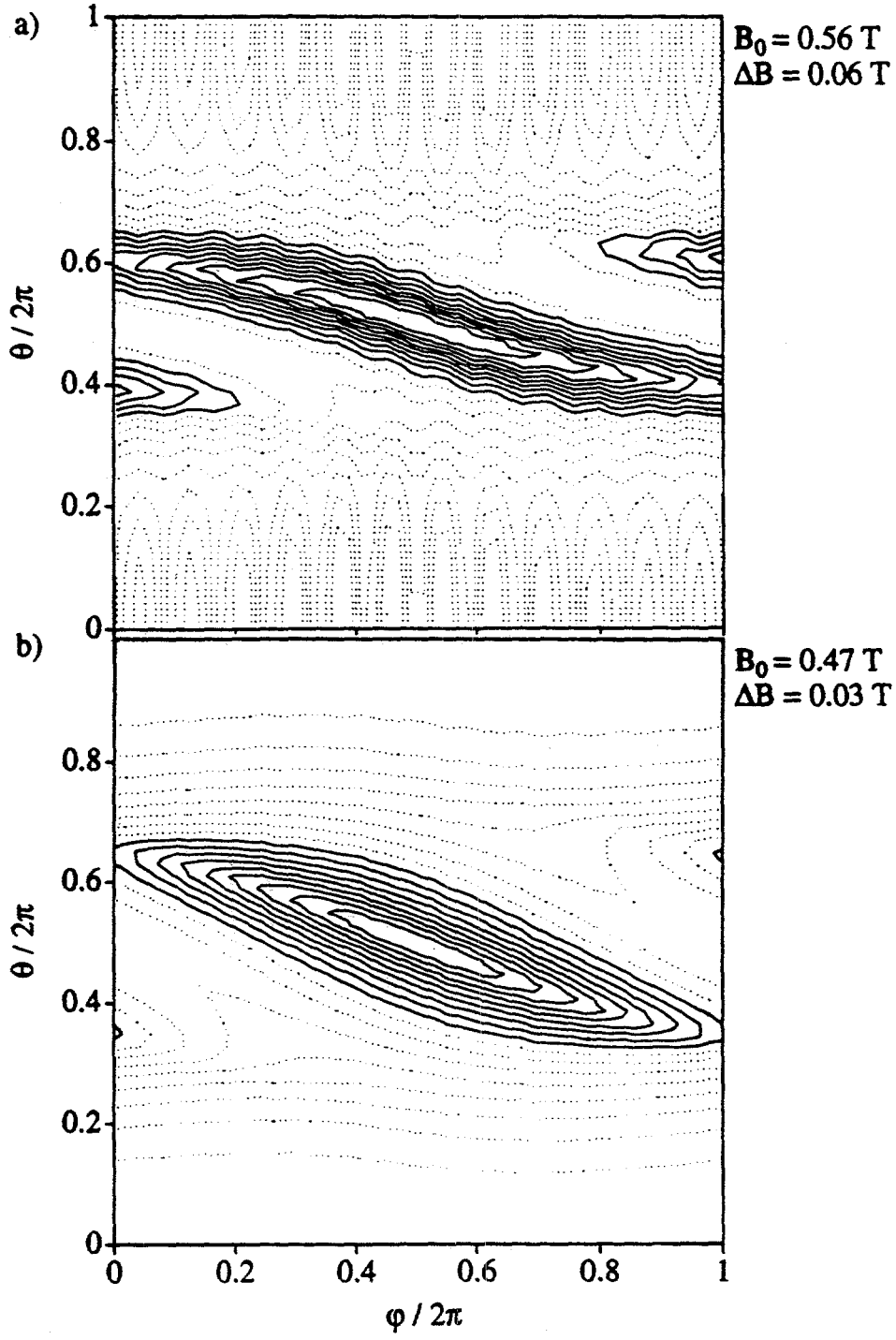

Fig. 7. (a) Distribution of |B| on flux surfaces; (a) flux surface $\rho = 1$, (b) $\rho = 0.5$. B_0 corresponds to the value of the first solid-line contour, and ΔB is the difference between the adjacent contours. Solid contours correspond to $|B| \geq B_0$, and dotted ones - to $|B| < B_0$.

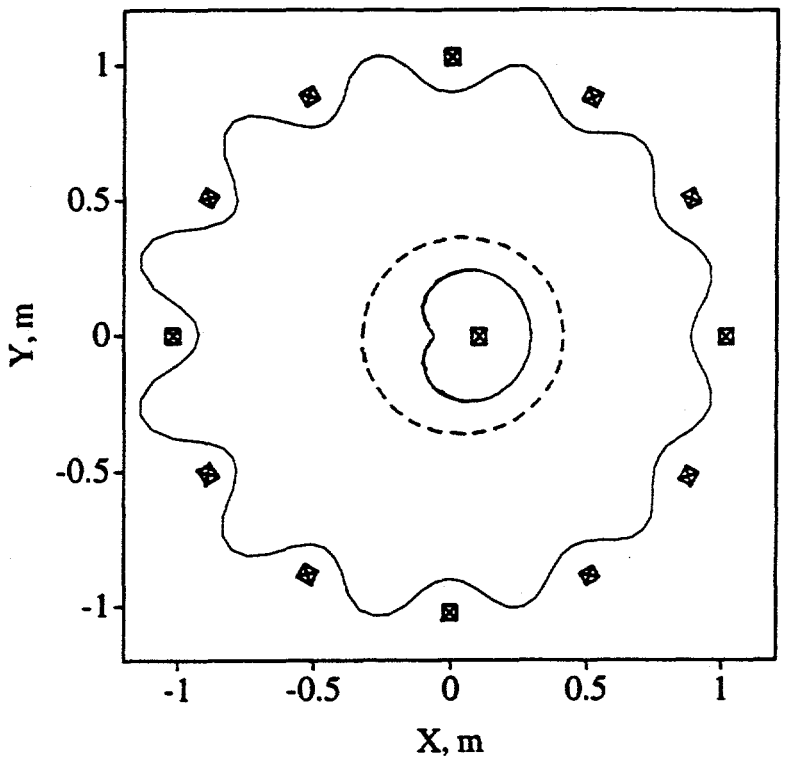

Fig. 8. The equatorial cross-section (Z = 0) of the plasma; the cross-sections of the TF coils and the HCP are presented as well. The magnetic axis projection is shown by the dashed curve.

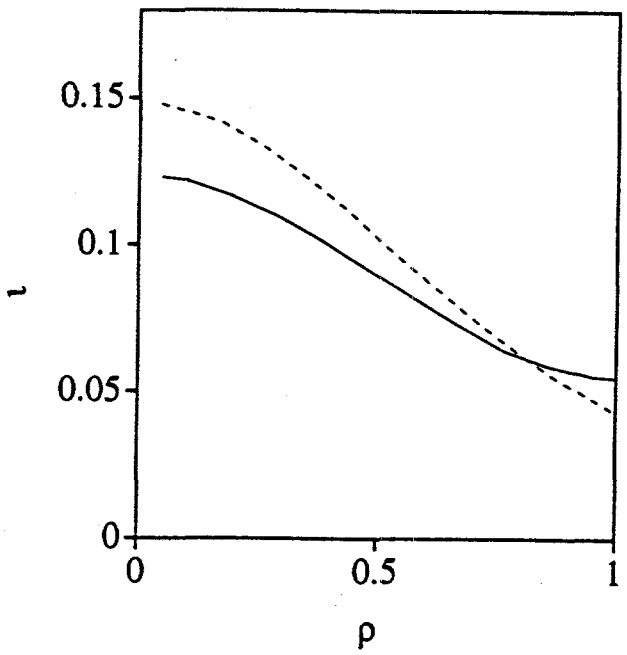

Fig. 9. Radial dependence of the rotational transform for the HPS without PF rings (solid curve), and with PF rings (dashed curve).

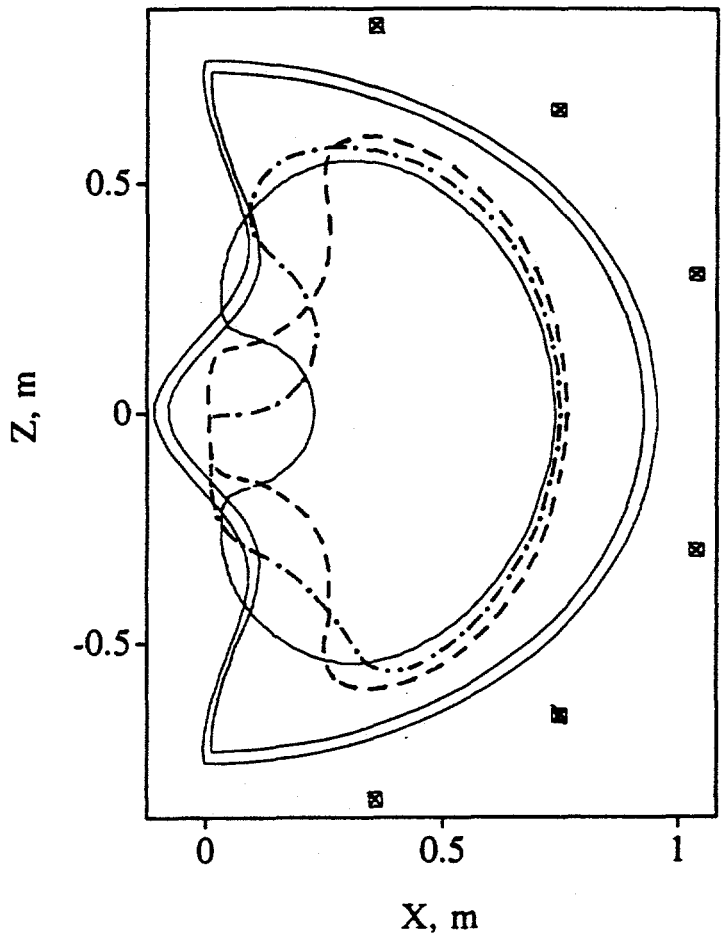

Fig. 10. Poloidal projection of the HPS coil configuration with PF rings, together with the main cross-sections of the last closed flux surface.

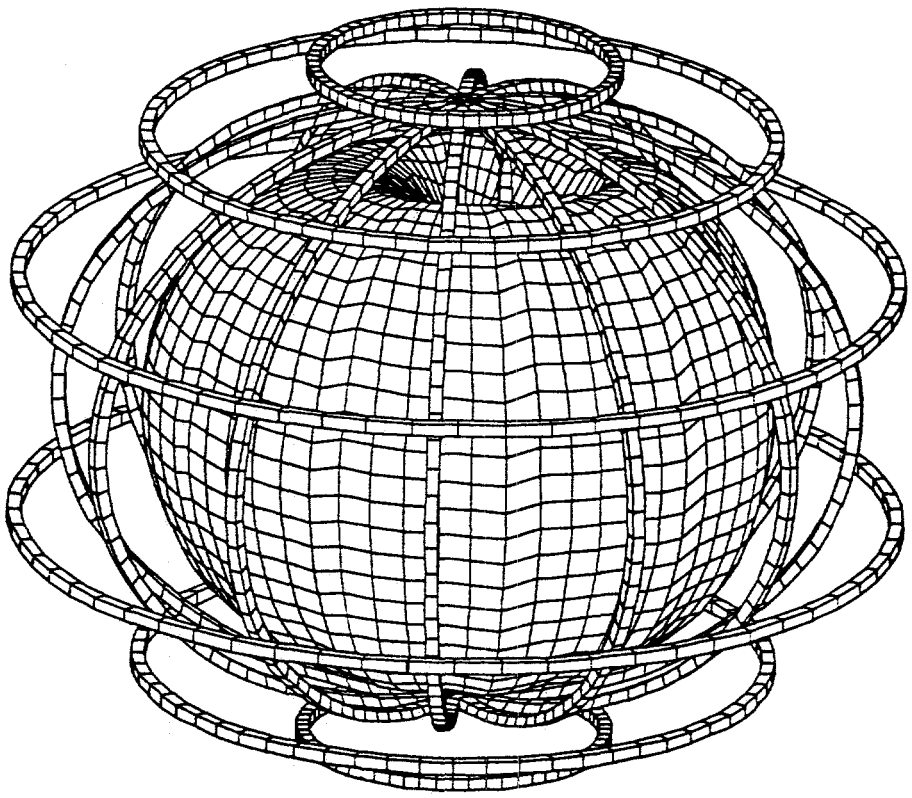

Fig. 11. Perspective view of the HPS plasma and the coils corresponding to the HPS configuration with PF rings of Fig. 10.

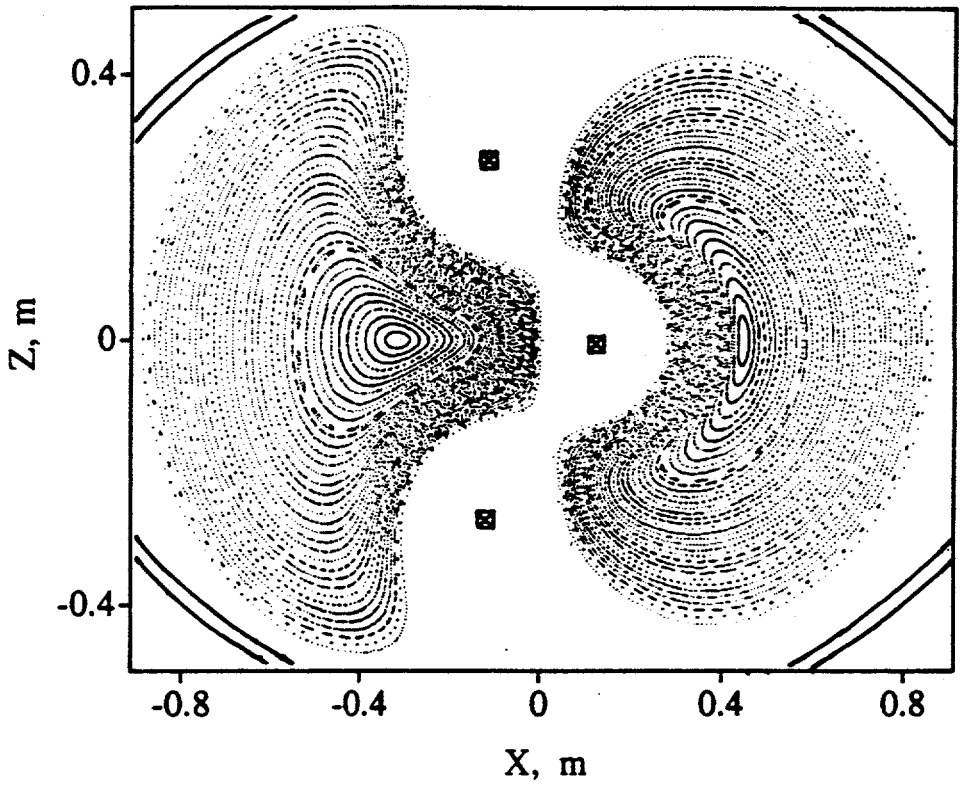

Fig. 12. Poincare puncture plots for the HPS configuration with PF rings. X-Z cross-section is shown.

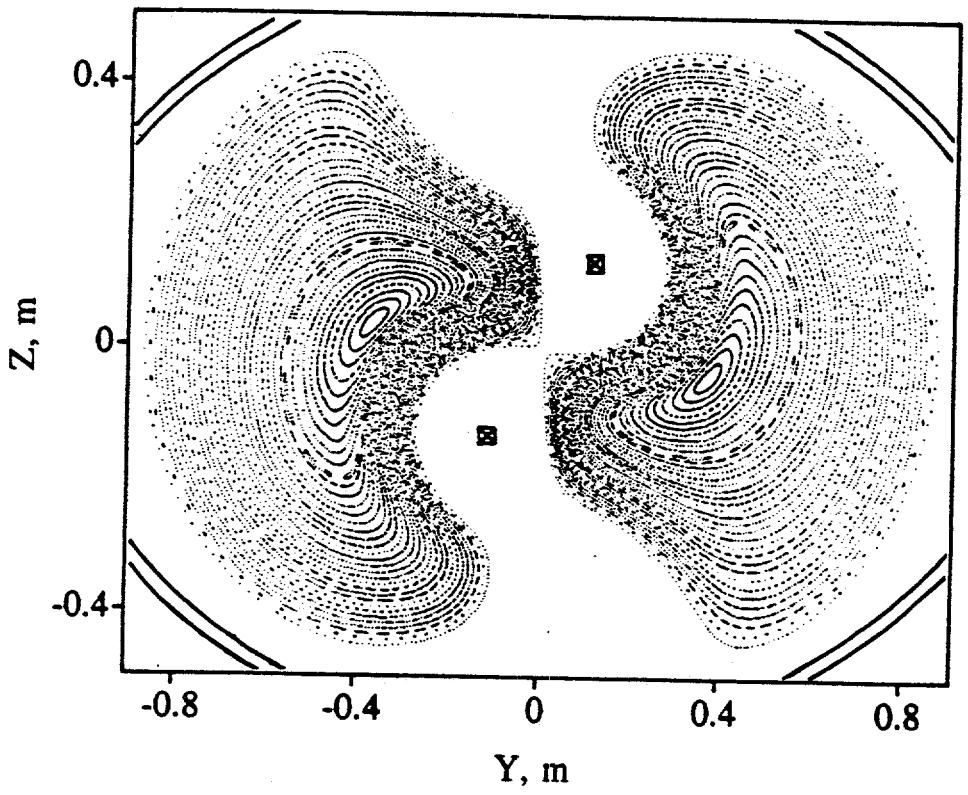

Fig. 13. Same as Fig. 12, but for the Y-Z cross-section.

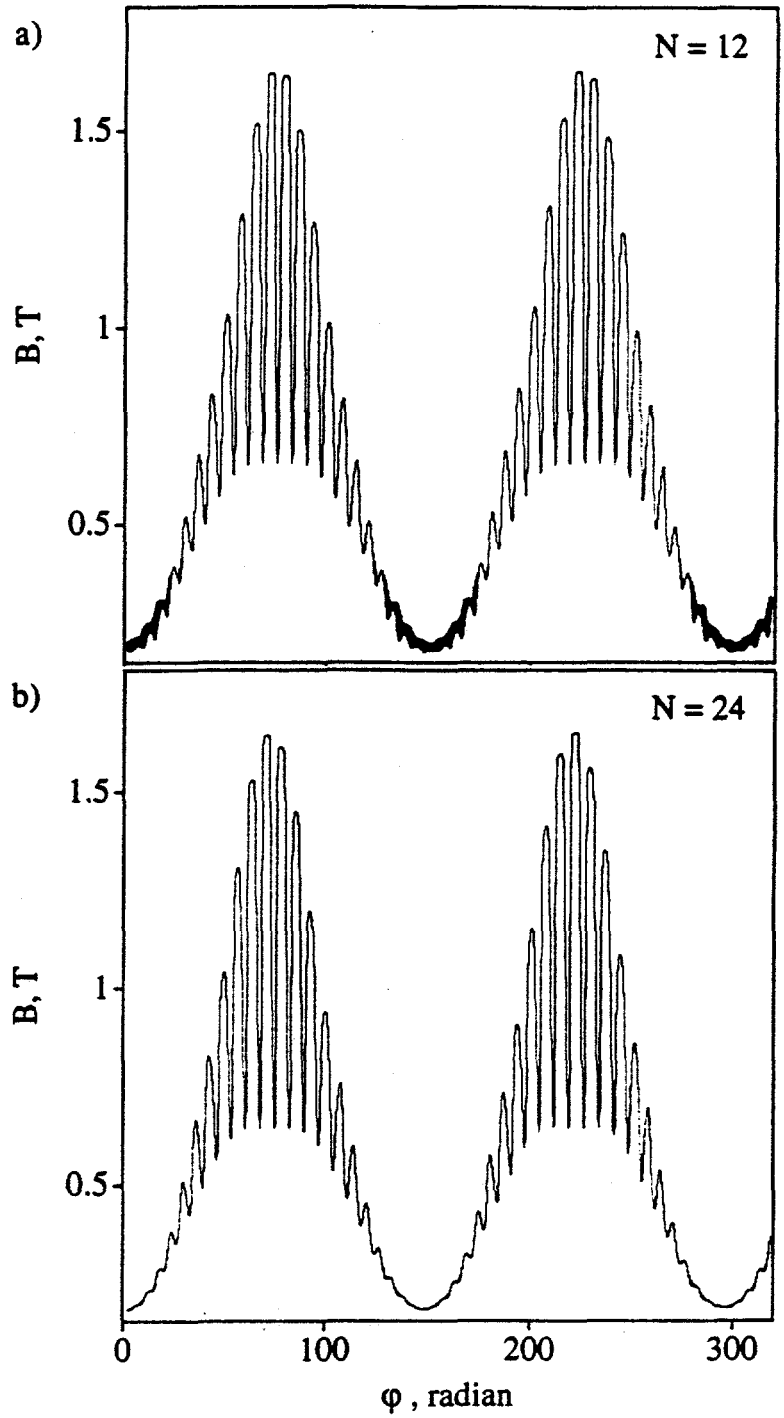

Fig. 14. Magnetic field variation along a field line for the last closed vacuum flux surface in the HPS configuration with PF rings; (a) with 12 TF coils, (b) with 24 TF coils.

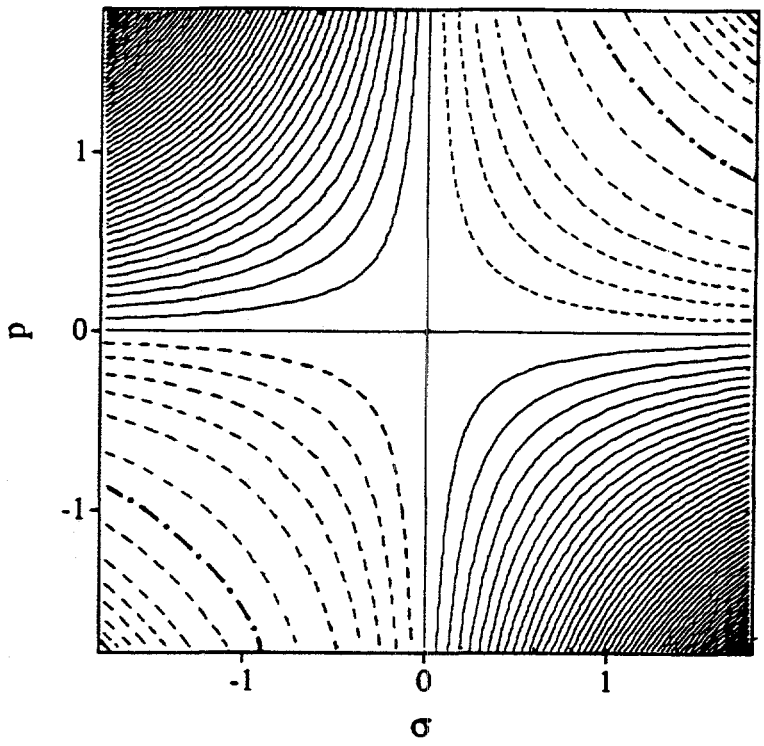

Fig. 15. Contours of S/S_o in a σ–p plane. Solid contours correspond to $S/S_o \geq 1$, and dashed ones to $S/S_o < 1$. The difference between neighboring contours is 0.15. The minimum of 0.066 is shown by the dash-dot lines.

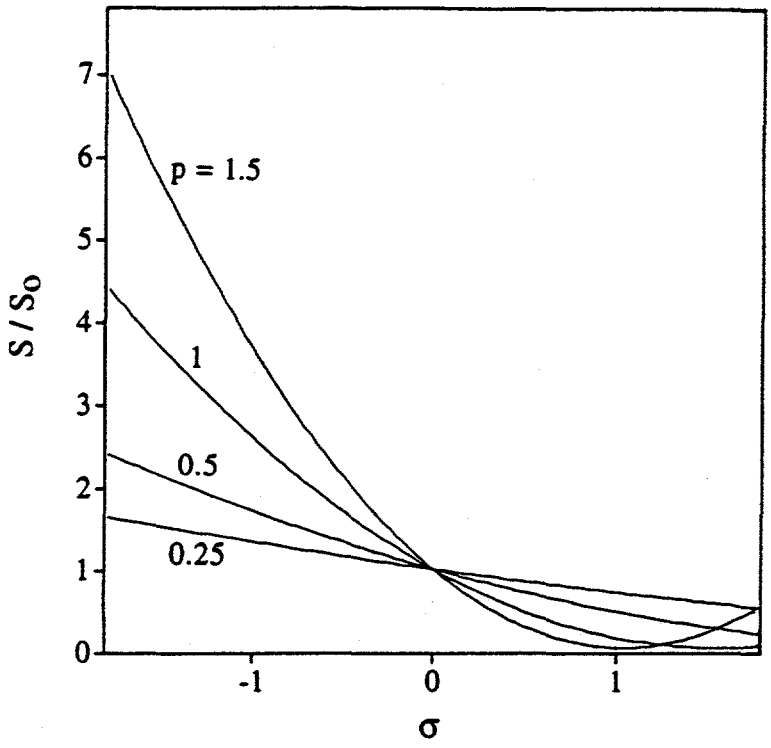

Fig. 16. S/S_o as a function of σ for 4 values of p.

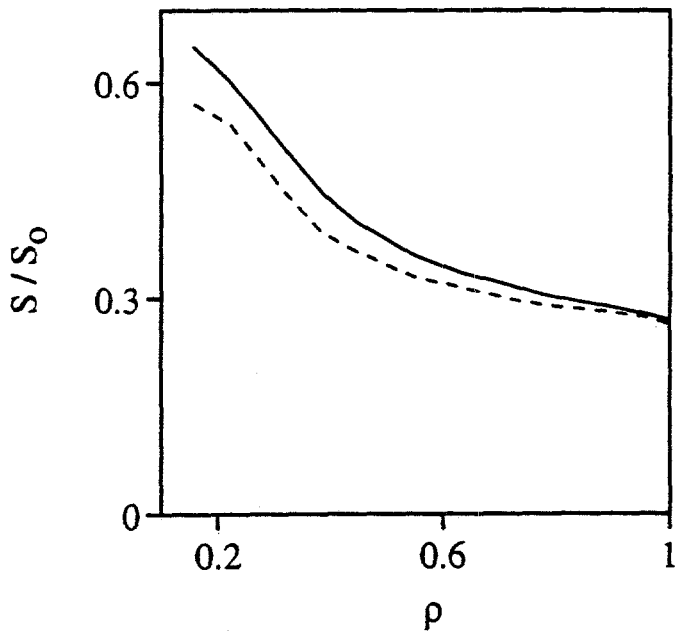

Fig. 17. Radial dependence of S/S_o for the HPS configurations without PF rings (solid line) and with PF rings (dashed).